nature communications

Article

https://doi.org/10.1038/s41467-025-65131-1

Presence of SARS-CoV-2 in fetal organs via intraamniotic infection

Received: 26 January 2025

Accepted: 7 October 2025

Published online: 21 November 2025

Check for updates

Shengnan Wu[1,4], Linchen Tang[1,2,4], Zeying Liu[1,4], Meijuan Wu[1], Xiaoying He[1], Shanshan Shan[1], Yicheng Zhou[1], Ke Lin[1], Qingxin Xu[1], Shidong Tan[1], Ziyi Zhang[1], Yao Xu[1,2], Cancan Wang[1], Feiye Zhu[3], Zhiyun Wei[1,2] ✉ & Liping Jin[1,2] ✉

The COVID-19 pandemic underlined the need to focus on women's health, particularly during pregnancy. Recent studies have shown that maternal SARS-CoV-2 infection during pregnancy may increase obstetrical risks. However, intraamniotic SARS-CoV-2 infection has been understudied. Here, we conduct inclusive autopsies on 18 fetuses following maternal SARS-CoV-2 infection to determine whether and which fetal organs can be infected by SARS-CoV-2 in utero. We analyze a total of 538 samples from 32 tissue types to comprehensively map and quantify the distribution and replication patterns of SARS-CoV-2 across fetal organs. Our observations reveal that SARS-CoV-2 can be widely distributed in fetal organs through vertical transmission. As the length of time from SARS-CoV-2 infection to termination of pregnancy increases, the prevalence of infection in fetal organs decrease. Further, proteomic profiling reveals DNA damage and immune imbalance in infected organs.

The global emergence of severe acute respiratory syndrome coronavirus 2 (SARS-CoV-2) has posed a significant threat to public health worldwide[1–3]. SARS-CoV-2 exhibits 79% nucleotide sequence homology with SARS-CoV and 50% with Middle-East respiratory syndrome coronavirus (MERS-CoV)[4]. It has been reported that infections with SARS-CoV or MERS-CoV during pregnancy may result in severe complications, including maternal mortality, spontaneous miscarriage, preterm delivery, and intrauterine growth restriction[5–9]. Recent studies have identified SARS-CoV-2 infection as a potential risk factor for pregnancy complications, as the incidence of clinical manifestations appears to be increased, including preterm birth and hypertensive disorders of pregnancy[10–14]. Several prospective observational cohort studies have also suggested that neonates born to mothers with symptomatic coronavirus disease 2019 (COVID-19) exhibit an elevated prevalence of neurological or neuropsychiatric abnormalities[15].

Therefore, growing concerns are being raised regarding the potential for mother-to-fetus transmission of SARS-CoV-2. Several existing studies suggest that newborns exhibit low rates of positivity or only show the presence of specific fetal IgM antibodies even when their mothers are infected with SARS-CoV-2 during pregnancy[16,17]. However, other cases have reported evidence of transplacental transmission of SARS-CoV-2 in neonates born to mothers infected in the last trimester, with high viral loads in placental tissues[12,18]. There was no direct evidence from autopsies of infected fetuses or comprehensive organ-specific viral analysis, and the precise transmission routes of congenital SARS-CoV-2 infection have not been adequately addressed.

In this work, to investigate the potential intraamniotic transmission of SARS-CoV-2 in pregnant women and identify vulnerable fetal organs susceptible to SARS-CoV-2 infection, we conduct fetal autopsies from 18 women experienced SARS-CoV-2 infection during pregnancy and 6 control ones without COVID-19 history. Women of both groups opted for second-trimester pregnancy termination due to either elective abortion or fetal abnormalities. A total of 634 fetal samples (538 from fetuses of women who were SARS-CoV-2 infected during pregnancy), from 32 tissue types, are collected and analyzed in this study. The coronavirus virion consists of nucleocapsid (N),

[1]Department of Integrated TCM-WM, Shanghai Key Laboratory of Maternal Fetal Medicine, Shanghai Institute of Maternal-Fetal Medicine and Gynecologic Oncology, Clinical and Translational Research Center, Shanghai First Maternity and Infant Hospital, School of Medicine, Tongji University, Shanghai, China. [2]Obstetrics & Gynecology Hospital of Fudan University, Shanghai Key Lab of Reproduction and Development, Shanghai Key Lab of Female Reproductive Endocrine Related Diseases, Shanghai, China. [3]Academy of Chinese Medical Sciences, Zhejiang Chinese Medical University, Zhejiang, China. [4]These authors contributed equally: Shengnan Wu, Linchen Tang, Zeying Liu. ✉e-mail: zhiyun_wei@163.com; jinlp01@163.com

membrane (M), envelope (E), and spike (S) proteins, which serve as structural components[4,19]. ORF3a (OR) is one of the accessory proteins encoded by SARS-CoV-2[20]. Therefore, we perform highly-sensitive droplet digital polymerase chain reaction (ddPCR) to detect and quantify the N gene of SARS-CoV-2 in fetal organs[21], followed by quantitative real-time PCR with reverse transcription (RT-qPCR) to detect subgenomic RNA, a reliable indicator of recent viral replication, thereby serving as a valuable marker in assessing viral activity[22]. Subsequently, RNA in situ hybridization (RNAscope) for SARS-CoV-2 OR, N, and S RNA is applied to validate the ddPCR findings. Transmission electron microscopy (TEM) is employed to confirm the presence of viral particles in fetal organs exhibiting high quantification of SARS-CoV-2 RNA (N) via ddPCR, while immunofluorescence (IF) is utilized for further validation of the associated SARS-CoV-2 proteins. Astral-data independent acquisition (DIA) proteomic profiling and analysis are applied to shed light on the biochemical pathways and biological processes modulated by SARS-CoV-2.

Results

Overview of the fetal autopsy cohort

Between 12 May 2022 and 8 June 2023, 24 pregnant Chinese Han women were recruited in Shanghai First Maternity and Infant Hospital, who opted for second-trimester pregnancy termination due to either elective abortion or fetal abnormalities. Among them, 18 were infected with SARS-CoV-2 during gestational weeks 4–21 (positive on both qPCR test and antigen test), and their pregnancy terminations were conducted 1–16 weeks after infection. The other 6 women were never infected during pregnancy, evidenced by routine qPCR test every 2–3 days. Within 6 h after abortion, fetal autopsies were collected on ice from 32 tissue types (2 female-specific ones, 1 male-specific one, and 29 common ones). Among the cohort of SARS-CoV-2 infections, a total of 538 samples were collected from 10 female fetuses and 8 male ones (Fig. 1a). According to the interval between termination and infection, we categorized autopsy cases into recent (≤4 weeks; n = 2), mid (≤12 weeks; n = 6) and long-ago (>12 weeks; n = 10) subgroups. The characteristics of the cohort data can be found in Supplementary Table 1.

Widespread fetal infection

Among 538 fetal samples, the SARS-CoV-2 RNA (N) was detected in 49 specimens (at least 5 copies per ng of total RNA), with relatively high quantification observed in 21 specimens (at least 10 copies per ng of total RNA) using highly sensitive ddPCR (Fig. 1b). It appeared that one recently infected woman transmitted the viral infection vertically to her fetus (S38), with the highest number of infected fetal organs. However, vertical transmission was not observed in the fetus from the other recently infected woman (S36). A small, sporadic number of organs exhibited SARS-CoV-2 infection in the fetuses of mid interval, while a lower number of infections were observed in fetal organs from women infected long ago. Among 32 examined tissue types, 16 were detected with high quantification of viral RNA, indicating widespread of fetal infections.

To investigate recent virus replication, subgenomic RNA of SARS-CoV-2 was detected across all 538 fetal specimens. Among them, 10 specimens exhibited high levels of subgenomic RNA quantification (Fig. 1b), which all were tested positive for SARS-CoV-2 RNA (N) accordantly.

Multi-layer validation of SARS-CoV-2 existence in fetal organs

We applied in situ hybridization on three SARS-CoV-2 RNAs (S, N and OR) using the RNAscope technology in fetal specimens. All three RNA targets were detected in all fetal specimens with high N copies based on ddPCR, except for the cerebellum sample from the fetus S20 (Fig. 2a–u and Supplementary Fig. 1). TEM analysis revealed discrete viral-like particles within the thyroid (fetus S6), kidney (fetus S38), and testis (fetus S38) samples, as shown in Fig. 2v–x, suggesting successful entry of intact virions. Subsequently, the presence of SARS-CoV-2 OR, N, and S proteins was visually identified in the corresponding thyroid, thymus and testis specimens (Fig. 3a and Supplementary Fig. 2). Histological analysis of the thyroid (fetus S6), kidney (fetus S38), and testis (fetus S38) samples revealed signs of necrosis and acute inflammatory infiltration (Supplementary Fig. 3). These findings provided conclusive evidence regarding the presence of SARS-CoV-2 in fetal organs during maternal infection.

Key proteins of SARS-CoV-2 infection were expressed in fetal organs

The entry of coronaviruses into host cells is mediated not solely by the interaction between the viral S proteins and cellular receptors (such as angiotensin-converting enzyme 2, ACE2), but also requires the priming of the S protein by host cell proteases[4,23]. In the context of SARS-CoV-2, the transmembrane serine protease 2 (TMPRSS2) plays a pivotal role in priming the SARS-CoV-2 S protein for fusion[23]. Hence, the analysis of ACE2 and TMPRSS2 staining was performed in the fetal specimens. Co-expression of ACE2 and TMPRSS2 was observed in fetal organs detected with viral RNAs and proteins (Fig. 3b). These findings validate fetal expression of the receptor and accessory protein of SARS-CoV-2, further ensuring the entry mechanism of SARS-CoV-2 into host cells.

Histological changes in infected fetal organs

SARS-CoV-2 N protein can increase the release of HMGB, one of the damage-associated molecular patterns, which may trigger M1 proinflammatory macrophage activation[24]. Hence, HMGB and immune cells markers, such as M1 proinflammatory macrophage markers CD86 and CD11B, were used to evaluate immune response in SARS-CoV-2 infected samples[25]. Notably, immunofluorescence experiments indicated that the infected thyroid, thymus, and testis samples exhibited a significant increase in HMGB, CD86 and CD11B expression compared to control samples (Fig. 4a). Additionally, compared to control, fibrosis-related protein fibronectin (FN) level was higher in infected samples (Fig. 4b). These results demonstrated a significant augmentation in both immune response and fibrosis following fetal organ infection, mirroring the observed patterns in adult patients with COVID-19[21].

Proteomic impact of SARS-CoV-2 infection on fetal organs

To delve deeper into the biochemical pathways and biological processes modulated by SARS-CoV-2, a comprehensive comparative Astral-DIA proteomic profiling was conducted in fetal organs, including small intestine, thyroid, and thymus (Fig. 5a and Supplementary Data 1). According to GSEA analysis, we noticed that there was remarkable repression on DNA repair signaling in all three infected fetal organs (Fig. 5b). The GSEA analysis showed provoked IL2/STAT5 signaling in small intestine and thymus of infected groups compared with the corresponding control (Fig. 5c).

Discussion

Pregnancy significantly increases the susceptibility to severe COVID-19, encompassing hospitalization, mechanical ventilation, and mortality rates compared to non-pregnant individuals[26]. SARS-CoV-2 infection during pregnancy is associated with adverse fetal outcomes, including preterm birth, stillbirth, small size for gestational age, and reduced birth weight[1,27,28]. Additionally, infants born to infected mothers face increased risks of neurobehavioral deficits, delayed motor skills and kidney damage[11,29,30]. Some cases have reported a high load of the SARS-CoV-2 virus in the placenta, amniotic fluid, neonatal blood, fetal-intravascular mononuclear cells, fetal lungs, and kidneys from pregnant women tested positive for COVID-19 in the first or third trimester[2,12,22,23,30]. Limitations of these evidences include the inability to completely rule out delivery infection and the fact that most are based on single case reports.

https://doi.org/10.1038/s41467-025-65131-1

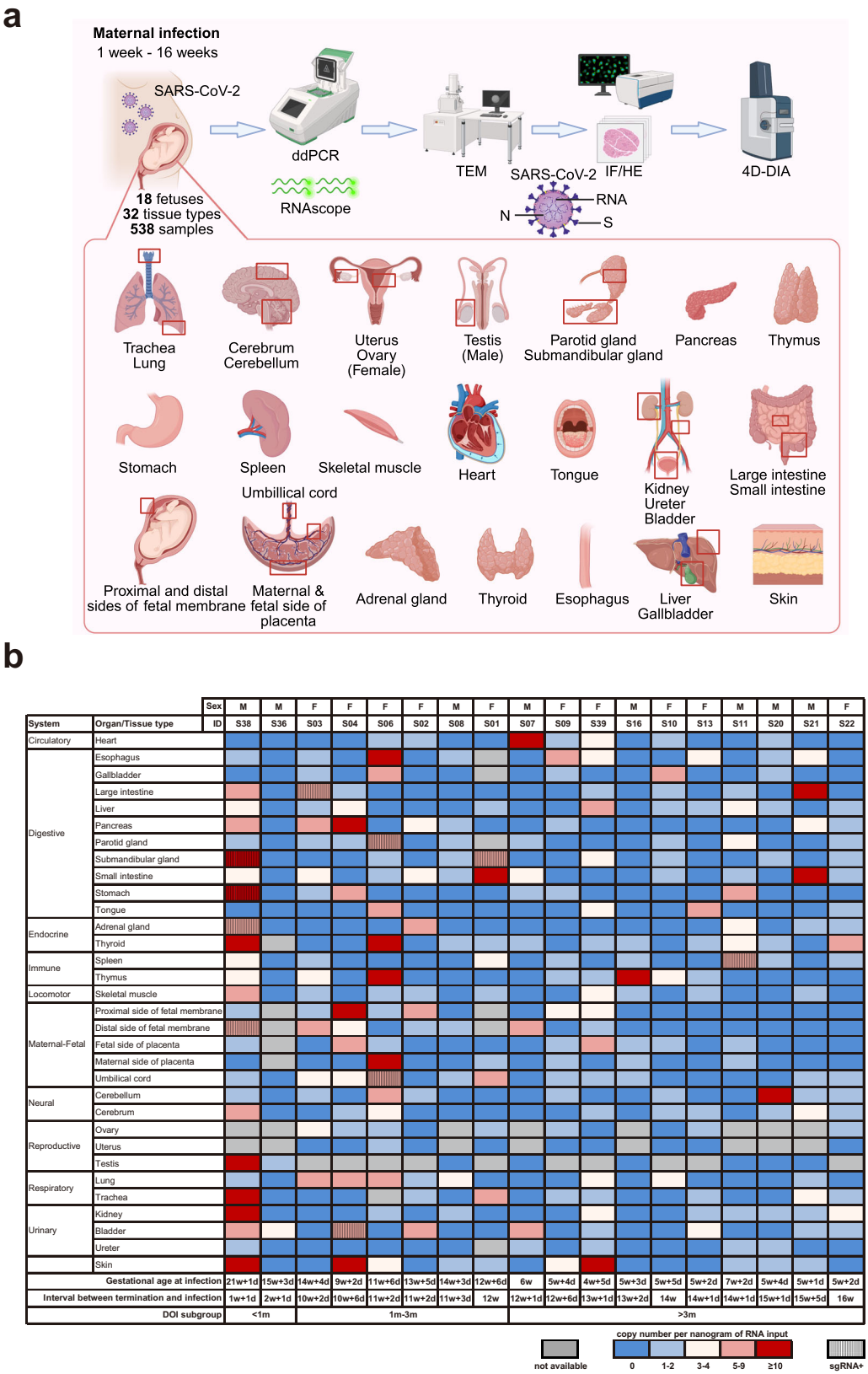

Fig. 1 | Overview of the cohort study and SARS-CoV-2 RNA quantification detected in 32 fetal organs. a Workflow of this study (created with BioRender.com). **b** Quantification of SARS-CoV-2 RNA in 538 fetal specimens using ddPCR. At the bottom of the figure, the samples were arranged in ascending order based on the duration of infection, from the shortest to the longest, prior to terminating pregnancy. According to the interval between termination and infection, the samples were grouped into early (≤4 weeks; n = 2), mid (≤12 weeks; n = 6) and late (>12 weeks; n = 10) subgroups. The organs were classified according to their respective body systems. ddPCR droplet digital polymerase chain reaction, TEM Transmission electron microscopy, IF Immunofluorescence, HE Hematoxylin and Eosin staining, 4D-DIA Astral-data independent acquisition proteomic, M male, F female. Source data are provided as a Source Data file.

https://doi.org/10.1038/s41467-025-65131-1

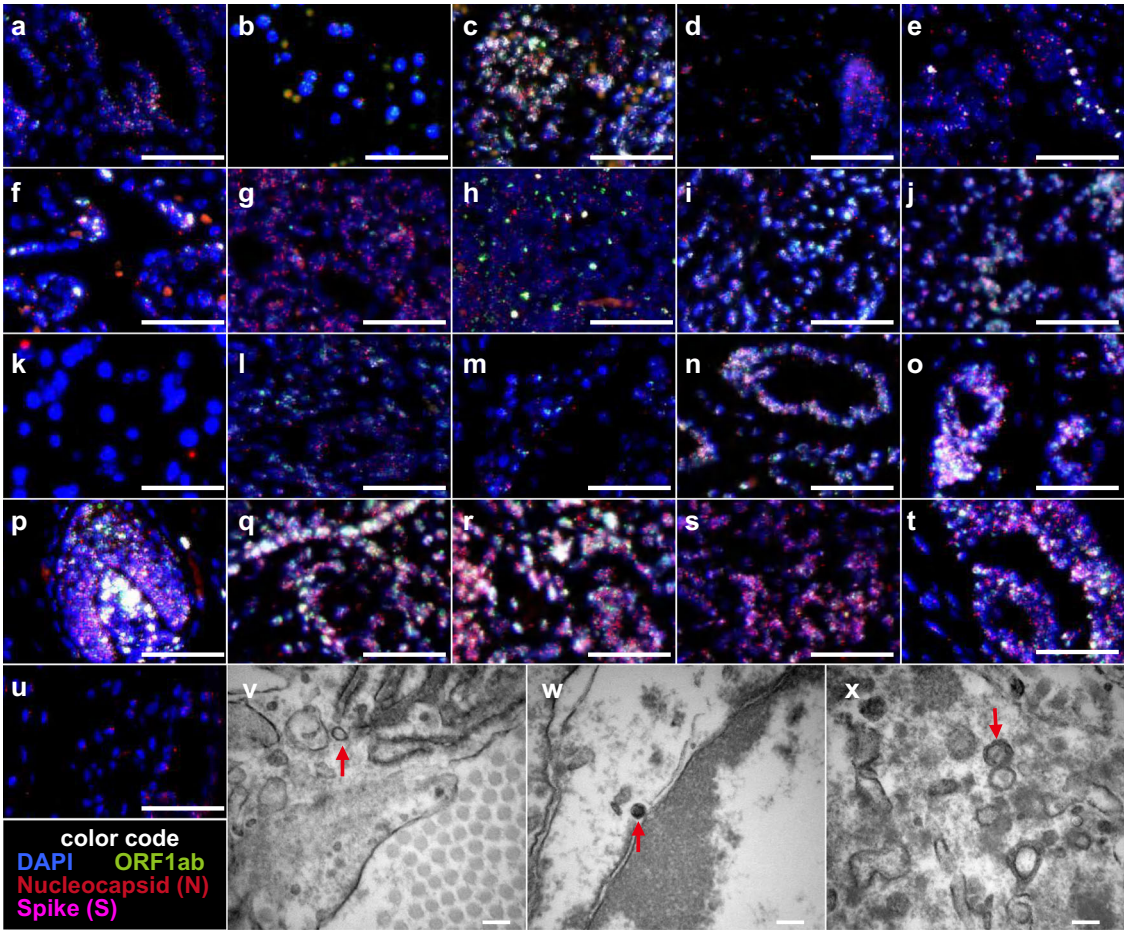

Fig. 2 | RNAscope and TEM of SARS-CoV-2 virus in fetal organs. SARS-CoV-2 RNA was verified by RNAscope in 21 fetal specimens, including small intestine of S01 (**a**), proximal side of fetal membrane of S04 (**b**), pancreas of S04 (**c**), skin of S04 (**d**), esophagus of S06 (**e**), maternal side of placenta of S06 (**f**), thyroid of S06 (**g**), thymus of S06 (**h**), heart of S07 (**i**), thymus of S16 (**j**), cerebellum of S20 (**k**), large intestine of S21 (**l**), small intestine of S21 (**m**), kidney of S38 (**n**), submandibular gland of S38 (**o**), skin of S38 (**p**), stomach of S38 (**q**), testis of S38 (**r**), thyroid of S38 (**s**), trachea of S38 (**t**), and skin of S39 (**u**). Scale bar, 50 μm. TEM analysis revealed the presence of virus-like particles (red arrows) in thyroid of S6 (**v**), kidney of S38 (**w**) and testis of S38 (**x**). Scale bar, 200 nm.

In this study, we present the most comprehensive analysis to date of the presence and quantification of SARS-CoV-2 across 32 fetal organs/tissue types, to our best knowledge. Among 538 fetal specimens, 49 were found to contain SARS-CoV-2 virus, with confirmed high viral load observed in 21 fetal specimens. In addition to previously reported infected maternal specimens such as placenta and umbilical cord, newly identified infected fetal organs included heart, esophagus, submandibular gland, stomach, pancreas, small intestine, large intestine, thyroid, thymus, testis and skin. These infected organs mainly involve the digestive, endocrine and immune systems. Considering the continuous ingestion of amniotic fluid by the fetus throughout gestation, it is plausible that the digestive system could be susceptible to infection from amniotic fluid. The thymus, being a vital lymphoepithelial organ, plays an indispensable role in facilitating the development and differentiation of T lymphocytes, particularly during the fetal period[31]. Consequently, it exhibits a close association with immune system maturation. The relatively high quantification of SARS-CoV-2 viral load in the thymus may lead to abnormal differentiation of T lymphocytes and affect immune system maturation. Additionally, the thyroid in the endocrine system is also heavily infected with a relatively high viral load. It plays a pivotal role in neural development. It has been speculated that neonates born to mothers exhibiting symptomatic COVID-19 displayed an elevated prevalence of neurological abnormalities[32,33]. However, in the 18 fetuses studied, only the cerebellum sample from donor S20 and the cerebrum sample from donor S38 were detected to harbor SARS-CoV-2 using ddPCR, with only the former exhibiting a high viral load. The validation of the cerebellum specimen using RNAscope yielded inconclusive results, suggesting that fetal brain organs exhibit limited susceptibility to SARS-CoV-2 infection. While no conclusive evidence is currently available for direct neural infection in the fetus, our findings, alongside existing literature, suggest that thyroid involvement might represent a potential mechanism for altered neurodevelopment. Given the established role of thyroid function in fetal brain development, these results highlight a need for further investigation into maternal SARS-CoV-2 infection and fetal thyroid health. In light of these observations, expanded screening for congenital hypothyroidism in infants born to mothers with antenatal infection might be warranted, particularly in regions where such screening is not yet routine[34,35].

SARS-CoV-2 infection can result in cytokine storm and inflammatory response in lungs, kidneys and other organs of COVID-19 patients[24,36]. Recently, studies on the activation or attenuation of the innate immune response and inflammation at the maternal-fetal interface following maternal infection with SARS-CoV-2 have shown varied results. Some investigations suggested that placentas with a high viral load exhibited substantial macrophage infiltration within the intervillous space, in contrast to uninfected controls[37,38]. However, other studies revealed that SARS-CoV-2 led to limited activation of immune cells, constrained antiviral response, and/or even enhanced immune tolerance at maternal-fetal interface[10]. Our data suggests that

https://doi.org/10.1038/s41467-025-65131-1

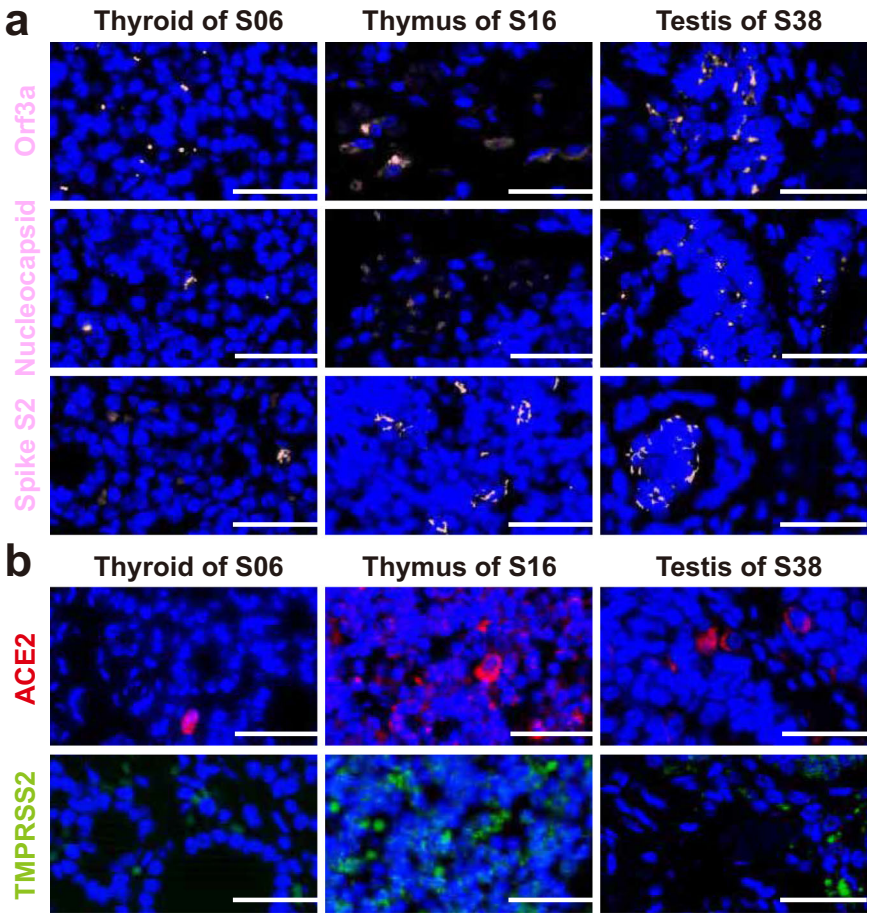

Fig. 3 | Expression of SARS-CoV-2 proteins and key human receptors for its entry in fetal organs. a IF detection of SARS-CoV-2 proteins. **b** IF staining of human proteins involved in SARS-CoV-2 entry mechanism. Scale bar, 50 μm. n = 2, 2 and 1 specimens for thyroid, thymus and testis, respectively. ACE2 angiotensin-converting enzyme 2, TMPRSS2 transmembrane serine protease 2.

an active immune response and fibrosis triggered by SARS-CoV-2 occurs in fetal organs with a high viral load. Moreover, our study identifies significant suppression of DNA repair signaling in the infected samples. It has been demonstrated that SARS-CoV-2 infection can cause DNA damage and additionally impede DNA repair through SARS-CoV-2 N-protein competitive binding with dilncRNAs[39]. The impinging on DNA damage response facilitates the replication of the virus and thus hinders the adaptive immune response, since an efficient and regulated DNA repair function is required for immunological diversification, especially for T and B cell receptor generation[40,41]. Proteomic profiling of infected fetal organs also highlights activation of IL2/STAT5 signaling. Repressed expression of IL2 was considered as one of the reasons that critical patients with COVID-19 pneumonia present with low $CD8^+$ T cell level[42]. During chronic viral infections, the augmenting IL2/STAT signaling rewires exhausted $CD8^+$ T cells and promotes Tex cell differentiation[43], which might be part of fetal antiviral immunity.

Surprisingly, among placentas of the 18 fetuses, only one fetal side of placenta (fetus S04) and one maternal side of placenta (fetus S06) were SARS-CoV-2 RNA (N) positive. Once SARS-CoV-2 reaches the placenta, it could cause placentitis and might cross the maternal-placental interface (either through infection of placental cells or through disruption of the placental barrier) to obtain access to fetal vessels, possibly reach the fetus and cause infection[44,45]. In our work, the pathogen was detected in only a few placentas. One possible reason was that we only collected a small piece of tissue (about 5-10 mm^3) from the whole placenta to perform ddPCR. There were spatial limitations as the sampling might not fully represent the overall viral load of the placenta. However, the histology of the infected placenta was indeed altered. Necrosis of the syncytiotrophoblast was present, and extensive intervillous fibrin was deposited in infected placentas (Supplementary Fig. 4). The disrupted placental barrier might allow SARS-CoV-2 in utero transmission.

In this study, among 18 fetuses, only 2 showed absolutely no sign of infection. It seemed that as the length of time from maternal SARS-CoV-2 infection to termination of pregnancy increased, the prevalence of SARS-CoV-2 infection in fetal organs decreased. Compared to adult organs, it was noteworthy yet understandable that the viral load in fetal organs appeared significantly lower. The sporadic nature of infections suggests that transmission occurs only under specific conditions, highlighting the protective role of the maternal-fetal barrier. Consequently, the likelihood of fetal infection is not conclusive and infected pregnant women should not be overly alarmed. Accordantly, most babies born to mothers with COVID-19 are asymptomatic or have mild disease[46,47].

The opportunistic cohort design constitutes the major weakness of our study. In this study, 21 donors were successfully recruited within a short timeframe, as only a few obstetrics & gynecology hospitals, including ours, remained operational during and shortly after the Shanghai lockdown. The time window for this study was narrow. Prior to the lifting of lockdown in June 2022, Shanghai reported minimal daily incidence of COVID-19, and no induced labor was performed on women who had experienced antenatal SARS-CoV-2 infection at our center. However, ~1 year after the lifting of lockdown, the discontinuation of widespread public testing made it impossible to determine infection status during pregnancy. We are

https://doi.org/10.1038/s41467-025-65131-1

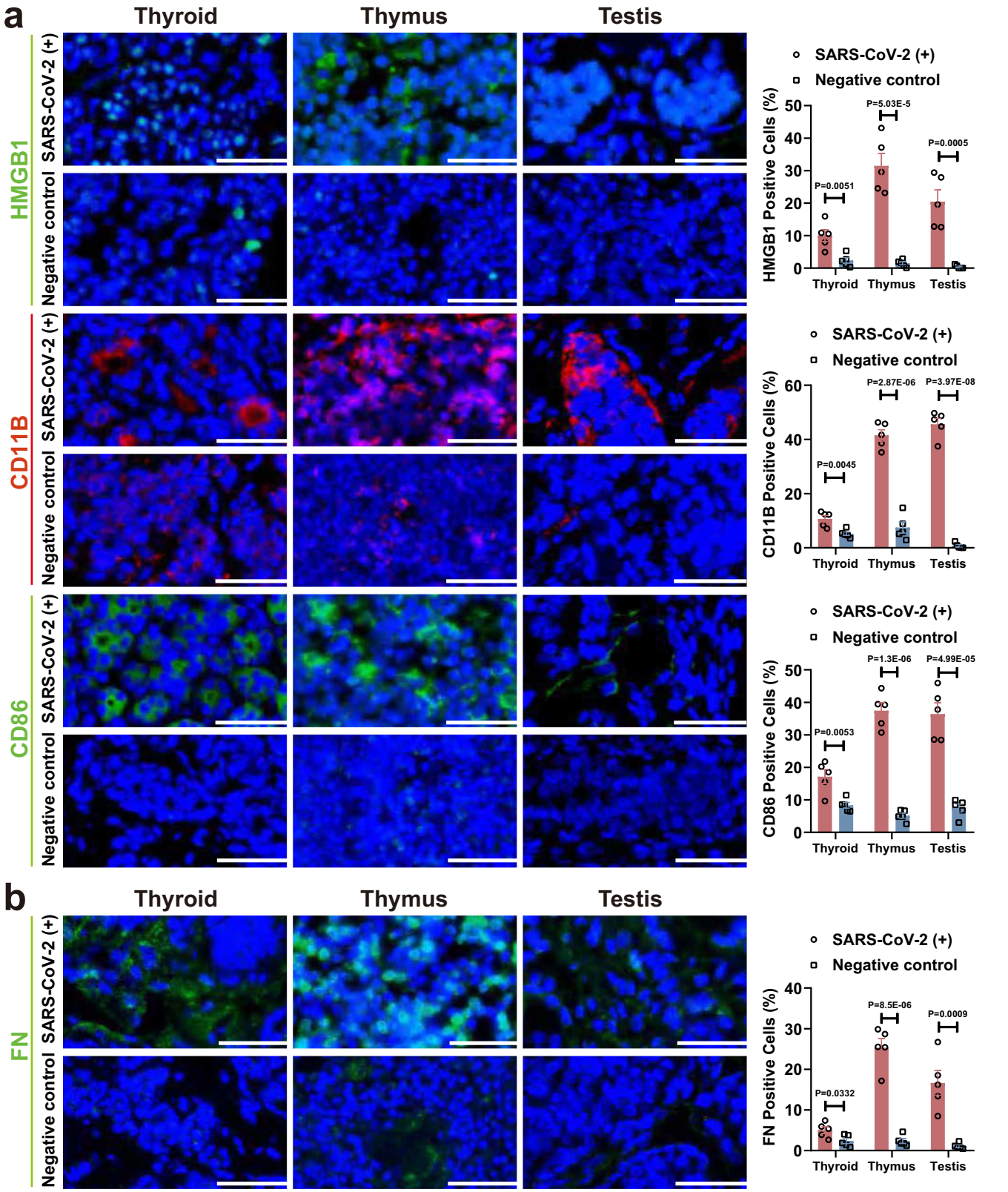

Fig. 4 | IF analysis of markers associated with induced inflammation and fibrosis in SARS-CoV-2-infected fetal organs. a IF staining of inflammatory indicators HMGB, CD11B and CD86. **b** IF staining of fibrosis indicator FN. SARS-CoV-2-infected thyroid, thymus and testis were from S06, S16 and S38, respectively. Scale bar, 50 μm. Right panels compare the percentage of cells positive on corresponding markers between infected and non-infected fetal organs. n = 5 vs 5 views; data are presented as mean ± s.e.m.; two-sided t-test. FN fibrosis-related protein fibronectin. Source data are provided as a Source Data file.

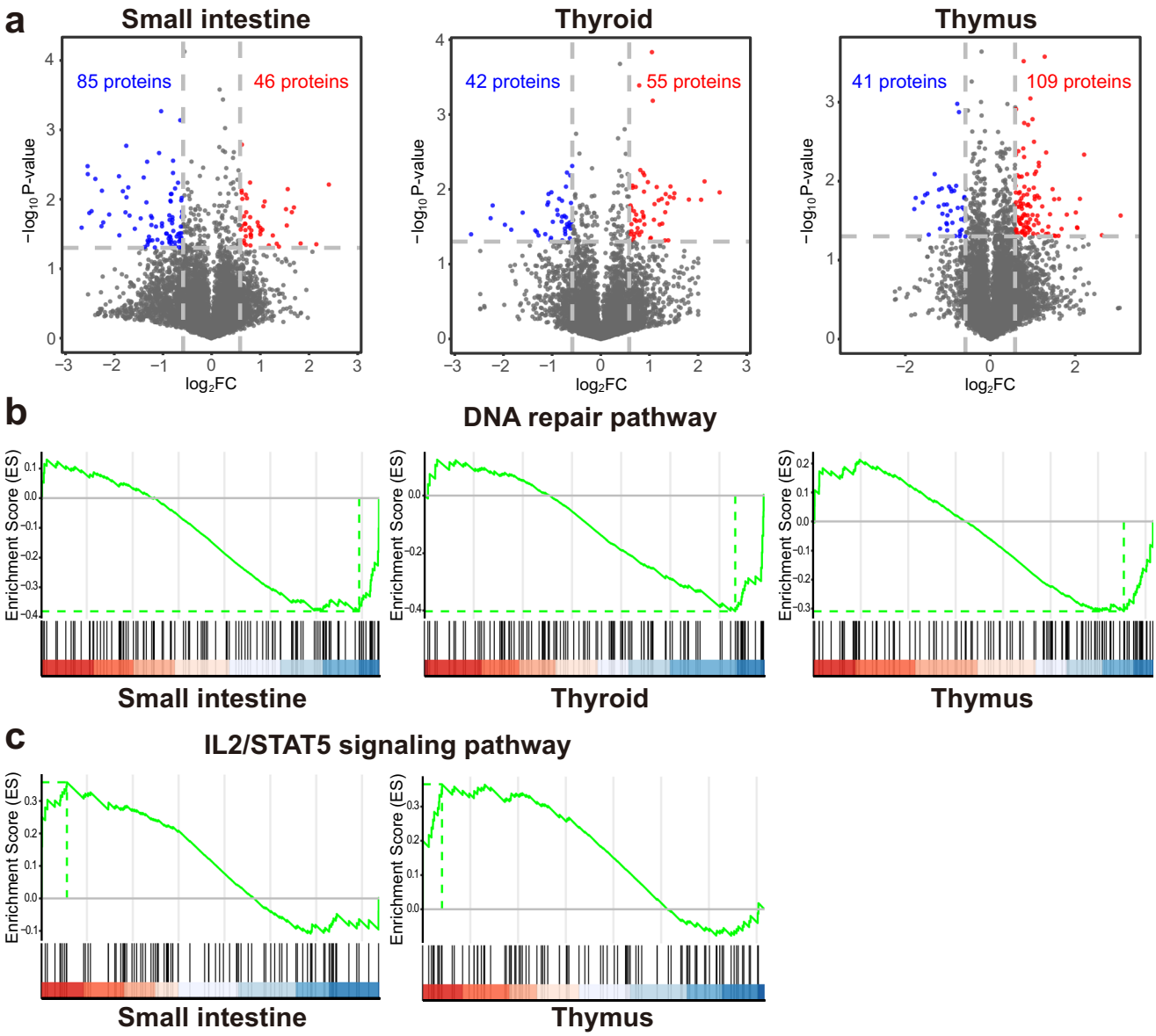

Fig. 5 | Proteomic alterations in SARS-CoV-2-infected fetal organs. a Volcano plots illustrating the differential protein expression profiles in small intestine, thyroid and thymus of infected fetuses (n = 2 vs 2 specimens). Unadjusted two-sided t-test. **b** GSEA analysis revealed a downregulation of DNA repair pathway in SARS-CoV-2-infected fetal organs. **c** The IL2/STAT5 signaling was upregulated in small intestine and thymus of fetuses with SARS-CoV-2 infection.

fortunate to have had the opportunity to design and conduct this study within a critical timeframe, enabling us to investigate the possibility of intraamniotic SARS-CoV-2 infection. Due to the small sample sizes of several discrete subpopulations, varying on period of infectivity, developmental stage at infection, and congenital anomalies, the certainty of the conclusions and the generalizability of our study are limited.

In summary, this study comprehensively examined the intraamniotic transmission of SARS-CoV-2 to fetal organs and revealed the persistent presence of the virus in multiple systems, even long after maternal infection. Although viral load in fetal organs appeared to be much lower than one in adult organs[21], both immunofluorescence and proteomics assays indicated significant affections of viral infection in local tissues. Due to the limitation of a relatively small sample size from a single center, further extensive validation and long-term follow-up studies are needed to elucidate the effects of fetal infection on postnatal development in children and adults.

Methods

Donor recruitment and sample collection

All autopsies were conducted with written informed consent from donors and the sample collections were approved by the Ethics Committee of the Shanghai First Maternity and Infant Hospital affiliated with Tongji University (permission numbers: KS2317, KS21343).

This study enrolled pregnant women from May 12, 2022 through June 6, 2023, who either had COVID-19 history during pregnancy (N = 18) or had never been infected (N = 6; Control donors). None of donors had COVID-19 history prior to her pregnancy. The COVID-19 history was determined by periodic PCR test ensured by local government. Donors' pregnancies were terminated in the second trimester due to voluntary induction of labor, chromosomal abnormalities, anatomical structural abnormalities or other reasons. At the time of pregnancy termination, donors were negative on COVID-19 PCR test. The demographics of the donors were summarized in Supplementary Table 1. Detailed macroscopic dissections were performed on ice to collect tissue samples from multiple organs within 6 h after induction

of labor (stored on ice), including proximal and distal sides of fetal membrane, fetal and maternal sides of placenta, umbilical cord, skin, heart, thymus, lung, gallbladder, liver, stomach, spleen, pancreas, small intestine, large intestine, ureter, bladder, kidney, adrenal gland, thyroid, trachea, esophagus, parotid gland, submandibular gland, tongue, cerebrum, cerebellum, skeletal muscle, uterus (female fetuses), ovary (female fetuses), and testis (male fetuses). Fresh tissues were snap frozen in liquid nitrogen and then stored at −80 °C for subsequent RNA extraction and data-independent acquisition proteomics assay. Tissues used for histopathologic/ISH analysis and transmission electron microscopy were freshly fixed with 10% neutral buffered formalin and 2.5% pentanediol for 24 h, respectively. All experiments were conducted by researchers who were negative on COVID-19 PCR test at the moment.

Digital droplet PCR (ddPCR) and subgenomic RNA analysis

Total RNA was isolated using a RNAprep Pure Tissue Kit (Tiangen Biotech, China) according to the manufacturer's protocols. The QuantStudio 3D Digital PCR System and QuantStudio 3D Digital Chip Kit v2 (Life Technologies, Carlsbad, CA, USA, A26316) were used to detect and quantify SARS-CoV-2 nucleocapsid RNA (forward primer: 5′-TTACAAACATTGGCCGCAAA-3′; reverse primer 5′-GCGCGACATTC CGAAGAA-3′; probe 5′-FAM-ACAATTTGCCCCCAGCGCTTCAG-BHQ1-3′)[48] and human GAPDH RNA (forward primer 5′-CAAGGCTGTGGG-CAAGGT-3′; reverse primer 5′-VIC-GGAAGGCCATGCCAGTGA-MGB-3′; probe 5′-ATCCCTGAGCTGAACG-3′; designed using Primer Express Software v3.0.1) of samples. The raw data was collected and analyzed using QuantStudio 3D Analysis Suite (version 1.0, Thermo Fisher Scientific). Results were then normalized to copies of the N gene per nanogram of RNA input. The sample must be positive for the human GAPDH gene under the manufacturer's limit of detection (LOD) with ≥4 copies per microliter to ensure successful RNA extraction and to be reported. After the background was removed according to the negative control samples, LOD of ≥5 copies per ng RNA input was considered to be SARS-CoV-2 N gene positive. To further detect the replicating virus generated during productive infection, we conducted one-step RT-qPCR assay targeting subgenomic RNA of the envelope (E) gene (Forward primer 5′-CGATCTCTTGTAGATCTGTTCTC-3′; Reverse primer 5′-ATATTGCAGCAGCACACA-3′; probe 5′-FAM-ACACTAGC-CATCCTTACTGCGCTTCG-BHQ1-3′)[49] using the One step RT-qPCR mix (Accurate Biotechnology, China, catalog no. RM0042) on a QuantStudio 5 Real-Time PCR system (version 1.3.1, Thermo Fisher Scientific). Primers and probes were synthesized by Thermo Fisher Scientific.

RNAscope in situ hybridization (ISH)

Tissues with SARS-CoV-2 N gene abundance higher than 10 copies per ng RNA were further submitted for RNA in situ hybridization using the RNAscope Multiplex Fluorescent Reagent Kit v2 (Advanced Cell Diagnostics, USA) according to manufacturer protocols. Briefly, formalin-fixed and paraffin-embedded (FFPE) tissue blocks were cut at 4 μm. After the sections were mounted on slides, the slides were air dried at room temperature overnight, then baked and deparaffinized. After deparaffinization, the slides were applied with RNAscope hydrogen peroxide followed by target retrieval using the steamer. Then the slides were incubated with protease at 40 °C for the amount of time specified by the tissue pretreatment recommendation provided by manufacturer. After the digestion, the slides were hybridized for 2 h at 40 °C in the HybEZOven with probe-V-nCov2019-S (Advanced Cell Diagnostics, catalog no. 848561), probe-V-nCoV2019-ORF1ab (Advanced Cell Diagnostics, catalog no. 895661) or probe-V-nCoV2019-N (Advanced Cell Diagnostics, catalog no. 846081). In addition, 3-plex Negative Control Probe (Advanced Cell Diagnostics, catalog no. 320871) and 3-plex Positive Control Probe (Advanced Cell Diagnostics, catalog no. 320861) were used as a negative and positive control, respectively. Then the slides were counterstained with DAPI and mounted. Images were acquired with an automatic digital slide scanner (PANNORAMIC MIDI, 3DHISTECH, Hungary) and presented in the form of merge layers.

Immunofluorescence

FFPE slides of different organs were technically supported by the Manual IHC kit (Akoya, NEL861001KT) according to manufacturer protocols. The following dilutions of primary antibody were used: SARS-CoV-2 nucleocapsid antibody (Cell Signaling Technology, 26369S, USA), 1:1000; SARS-CoV2 orf3a antibody (Novus Biologicals, NBP3-15985, USA), 1:1000; SARS-CoV-2 Spike Glycoprotein S2 antibody (Novus Biologicals, NB100-56578SS), 1:1000; ACE2 antibody (Proteintech, 21115-1-AP), 1:1000; TMPRSS2 antibody (Proteintech, 14437-1-AP), 1:1000; HMGB1 antibody (Proteintech, 10829-1-AP), 1:1000; CD11B antibody (Novus Biologicals, NB110-89474SS), 1:1000; CD86 antibody (Affinity Bioscience, DF6332, China), 1:1000; Fibronectin (FN) antibody (Proteintech, 66042-1-Ig), 1:1000 for IF staining. After incubated with secondary antibodies, the signal was amplified using the fluorophore-conjugated tyramide amplification system (PerkinElmer, USA), followed by counterstaining with DAPI. Slides were scanned by an automatic digital slide scanner (PANNORAMIC MIDI). Positive cells were automatically counted using the Halo software (version 3.4.2986, Lndica Labs, USA).

Transmission electron microscopy (TEM)

A transmission electron microscope was used to detect virus-like particles in fetal organs. Tissues fixed in 2.5% pentanediol were washed, dehydrated, embedded and polymerized. Then the tissue blocks were cut to 70 nm thin and fished out onto the copper screen. Images were observed and captured by a H7650TEM (HITACHI, Japan) using RADIUS software (version 2.1, EMSIS GmbH, Germany).

Hematoxylin and Eosin (H&E) staining

FFPE slides of different organs were subjected to standard Hematoxylin and Eosin (H&E) staining for the detection of histological changes. Slides were deparaffinized, stained with H&E, and then subjected to a digital pathological section scanner (KFBIO, KF-PRO-400-HI). K-Viewer was used to determine lesion area in different sections.

Astral-DIA proteomic profiling

A total of 12 samples were analyzed (n = 2 vs 2 in each of three organs). Proteins were extracted by SDT (4% SDS, 100 mM Tris-HCl, pH 7.6) lysis buffer and quantified using a BCA Protein Assay Kit (Beyotime, China). DTT (final concentration at 40 mM) was added to each sample and mixed at 600 rpm for 1.5 h (37 °C). After the samples cooled to room temperature, IAA (final concentration at 20 mM) was added into the mixture to block reduced cysteine residues and the samples were incubated for 30 min in darkness. Next, the samples were transferred to the filters (Microcon units, 10 kDa). The filters were washed with 100 μl UA buffer three times and then 100 μl 25 mM NH_4HCO_3 buffer twice. Finally, trypsin was added to the samples (trypsin: protein (wt/wt) ratio was 1:50) and incubated at 37 °C for 15–18 h (overnight), and the resulting peptides were collected as a filtrate. The peptides of each sample were desalted on C18 Cartridges (Empore SPE Cartridges MCX, 30 μm, Waters), concentrated by vacuum centrifugation and reconstituted in 40 μl of 0.1% (v/v) formic acid. The peptide content was estimated by UV light spectral density at 280 nm. The iRT standard peptide was added to peptide segments. The peptides from each sample were analyzed by Orbitrap Astral mass spectrometer (Thermo Scientific) connected to an Vanquish Neo system liquid chromatography (Thermo Scientific) in the data independent acquisition (DIA) mode. Precursor ions were scanned at a mass range of 380–980 m/z, MS1 resolution was 240,000 at 200 m/z, Normalized AGC Target: 500%, Maximum IT: 5 ms. 299 windows were set for DIA mode in

MS2 scanning, Isolation Window: 2 m/z, HCD Collision Energy: 25 eV, Normalized AGC Target: 500%, Maximum IT: 3 ms. DIA data was analyzed with DIA-NN 1.8.1. Main software parameters were set as follows: the enzyme as trypsin, the max miss cleaning site as 1, the fixed modification as Carbammimethyl (C), the dynamic modification was set to Oxidation (M) and Acetyl (Protein N-term), and the protein identified by database retrieval must pass the set filtering parameter FDR < 1%. The database was downloaded at website: http://www.uniprot.org. The input of GSEA is a protein expression matrix, in which the samples are divided into two groups, and the differentially expressed proteins between the two groups are found, and then sorted according to fold change to indicate the changing trend of protein expression between the two groups. The cluster profile package in R package (v4.4.4) was used in analysis.

Statistical analysis

Statistical analysis was performed using Graphpad Prism (version 9.0, GraphPad Software, USA). The Student's t test was applied for comparison between independent groups. All data are presented as mean ± s.e.m. $P < 0.05$ was considered statistically significant.

Reporting summary

Further information on research design is available in the Nature Portfolio Reporting Summary linked to this article.

Data availability

The mass spectrometry proteomics data generated in this study have been deposited in the ProteomeXchange Consortium via the iProX partner repository under accession code PXD058679 (https://www.iprox.cn/page/PSV023.html;?url=1750929934172Yrjy; Password: WjYx). The processed proteomics data are available at Supplementary Data 1. Negative controls for RNAscope and IF are available in Supplementary Figs. 1 and 2. Source data are provided with this paper.

References

1. Male, V. SARS-CoV-2 infection and COVID-19 vaccination in pregnancy. *Nat. Rev. Immunol.* **22**, 277–282 (2022).
2. Valdespino-Vázquez, M. Y. et al. Fetal and placental infection with SARS-CoV-2 in early pregnancy. *J. Med. Virol.* **93**, 4480–4487 (2021).
3. Shukla, V. V. et al. Social distancing during the COVID-19 pandemic and neonatal mortality in the US. *JAMA Netw. Open* **7**, e2422995 (2024).
4. Jackson, C. B., Farzan, M., Chen, B. & Choe, H. Mechanisms of SARS-CoV-2 entry into cells. *Nat. Rev. Mol. Cell Biol.* **23**, 3–20 (2022).
5. Adam, S. et al. Coronavirus and pregnancy: the challenges of the 21(st) century: a review. *Front. Microbiol.* **13**, 923546 (2022).
6. Pradhan, J., Mallick, S., Mishra, N., Tiwari, A. & Negi, V. D. Pregnancy, infection, and epigenetic regulation: A complex scenario. *Biochim. Biophys. Acta Mol. Basis Dis.* **1869**, 166768 (2023).
7. Álvarez-Del Río, B. et al. Nationwide analysis of COVID-19 complications, outcomes, and costs of childbirth in Spain. *Front. Med.* **12**, 1548245 (2025).
8. Sandoval, M. N. et al. COVID-19 infection history as a risk factor for early pregnancy loss: results from the electronic health record-based Southeast Texas COVID and Pregnancy Cohort Study. *BMC Med.* **23**, 274 (2025).
9. Perelli, F. et al. Preterm birth and SARS-CoV-2: does a correlation exist? *Biomedicines* **13**, https://doi.org/10.3390/biomedicines13020282 (2025).
10. Xi, C. et al. Immune rebalancing at the maternal-fetal interface of maternal SARS-CoV-2 infection during early pregnancy. *Protein Cell* **15**, 460–473 (2024).
11. Yates, E. F. & Mulkey, S. B. Viral infections in pregnancy and impact on offspring neurodevelopment: mechanisms and lessons learned. *Pediatr. Res.* **96**, 64–72 (2024).
12. Zia, M. T. K. et al. Vertical transmission of SARS-CoV-2 delta-variant in a preterm infant. *BMC Infect. Dis.* **24**, 537 (2024).
13. Celewicz, A. et al. SARS CoV-2 infection as a risk factor of pre-eclampsia and pre-term birth. An interplay between viral infection, pregnancy-specific immune shift and endothelial dysfunction may lead to negative pregnancy outcomes. *Ann. Med.* **55**, 2197289 (2023).
14. Dumitriu, D. & Gyamfi-Bannerman, C. Understanding risk for newborns born to SARS-CoV-2-positive mothers. *Jama* **325**, 2051–2052 (2021).
15. Prochaska, E., Jang, M. & Burd, I. COVID-19 in pregnancy: placental and neonatal involvement. *Am. J. Reprod. Immunol.* **84**, e13306 (2020).
16. Dong, L. et al. Possible vertical transmission of SARS-CoV-2 from an infected mother to her newborn. *Jama* **323**, 1846–1848 (2020).
17. Prabhu, M. et al. Pregnancy and postpartum outcomes in a universally tested population for SARS-CoV-2 in New York City: a prospective cohort study. *Bjog* **127**, 1548–1556 (2020).
18. Bouachba, A. et al. Placental lesions and SARS-Cov-2 infection: diffuse placenta damage associated to poor fetal outcome. *Placenta* **112**, 97–104 (2021).
19. Watanabe, Y., Allen, J. D., Wrapp, D., McLellan, J. S. & Crispin, M. Site-specific glycan analysis of the SARS-CoV-2 spike. *Science* **369**, 330–333 (2020).
20. López-Ayllón, B. D. et al. Metabolic and mitochondria alterations induced by SARS-CoV-2 accessory proteins ORF3a, ORF9b, ORF9c and ORF10. *J. Med. Virol.* **96**, e29752 (2024).
21. Stein, S. R. et al. SARS-CoV-2 infection and persistence in the human body and brain at autopsy. *Nature* **612**, 758–763 (2022).
22. Cuesta, G. et al. Utility of SARS-CoV-2 subgenomic RNA in kidney transplant recipients receiving remdesivir. *Infect. Dis. Ther.* **13**, 1703–1713 (2024).
23. Beesley, M. A. et al. COVID-19 and vertical transmission: assessing the expression of ACE2/TMPRSS2 in the human fetus and placenta to assess the risk of SARS-CoV-2 infection. *BJOG* **129**, 256–266 (2022).
24. Wu, W. et al. SARS-CoV-2 N protein induced acute kidney injury in diabetic db/db mice is associated with a Mincle-dependent M1 macrophage activation. *Front. Immunol.* **14**, 1264447 (2023).
25. Feng, C. et al. A novel PDPN antagonist peptide CY12-RP2 inhibits melanoma growth via Wnt/β-catenin and modulates the immune cells. *J. Exp. Clin. Cancer Res.* **43**, 9 (2024).
26. Carlson, J. et al. Pre-delta, delta, and omicron periods of the coronavirus disease 2019 (COVID-19) pandemic and health outcomes during delivery hospitalization. *Obstet. Gynecol.* **143**, 131–138 (2024).
27. Gurol-Urganci, I. et al. Maternal and perinatal outcomes of pregnant women with SARS-CoV-2 infection at the time of birth in England: national cohort study. *Am. J. Obstet. Gynecol.* **225**, 522.e521–522.e511 (2021).
28. Günther, J. et al. Variability in COVID-19 symptom presentation during pregnancy and its impact on maternal and infant outcomes across the pandemic. *Int. J. Infect. Dis.* 107157. https://doi.org/10.1016/j.ijid.2024.107157 (2024).
29. He, Z. et al. Vertical transmission and kidney damage in newborns whose mothers had coronavirus disease 2019 during pregnancy. *Int J. Antimicrob. Agents* **57**, 106260 (2021).
30. Creisher, P. S. & Klein, S. L. Pathogenesis of viral infections during pregnancy. *Clin. Microbiol. Rev.* **37**, e0007323 (2024).
31. Li, L. et al. Thymic microenvironment's impact on immunosenescence. *Immunol. Res.* https://doi.org/10.1007/s12026-024-09519-z (2024).
32. Kurokawa, M. et al. Neurological and neuroradiological manifestations in neonates born to mothers with coronavirus disease 2019. *Pediatr. Neurol.* **141**, 9–17 (2023).

33. Vivanti, A. J. et al. Transplacental transmission of SARS-CoV-2 infection. *Nat. Commun.* **11**, 3572 (2020).
34. Smith, A. A., Vesey, A., Helfrich, C. & Pasternak, J. A. Late gestation fetal hypothyroidism alters cell cycle regulation across multiple organ systems. *BMC Vet. Res.* **20**, 268 (2024).
35. Salas-Lucia, F. Mapping thyroid hormone action in the human brain. *Thyroid* **34**, 815–826 (2024).
36. Ahmad, F., Keshri, V. & Singh, S. K. ORF3a of SARS-CoV-2 modulates PI3K/AKT signaling in human lung epithelial cells via hsa-miR-155-5p. *Int J. Biol. Macromol.* **268**, 131734 (2024).
37. Shook, L. L. et al. Maternal SARS-CoV-2 impacts fetal placental macrophage programs and placenta-derived microglial models of neurodevelopment. *J. Neuroinflammation* **21**, 163 (2024).
38. Schwartz, D. A. & Morotti, D. Placental pathology of COVID-19 with and without Fetal and Neonatal Infection: trophoblast necrosis and chronic histiocytic intervillositis as risk factors for transplacental transmission of SARS-CoV-2. *Viruses* **12**, https://doi.org/10.3390/v12111308 (2020).
39. Gioia, U. et al. SARS-CoV-2 infection induces DNA damage, through CHK1 degradation and impaired 53BP1 recruitment, and cellular senescence. *Nat. Cell Biol.* **25**, 550–564 (2023).
40. Wang, Y., Abolhassani, H., Hammarström, L. & Pan-Hammarström, Q. SARS-CoV-2 infection in patients with inborn errors of immunity due to DNA repair defects. *Acta Biochim. Biophys. Sin.* **54**, 836–846 (2022).
41. Grand, R. J. SARS-CoV-2 and the DNA damage response. *J. Gen. Virol.* **104**, https://doi.org/10.1099/jgv.0.001918 (2023).
42. Shi, H. et al. The inhibition of IL-2/IL-2R gives rise to CD8(+) T cell and lymphocyte decrease through JAK1-STAT5 in critical patients with COVID-19 pneumonia. *Cell Death Dis.* **11**, 429 (2020).
43. Beltra, J. C. et al. Stat5 opposes the transcription factor Tox and rewires exhausted CD8(+) T cells toward durable effector-like states during chronic antigen exposure. *Immunity* **56**, 2699–2718.e2611 (2023).
44. Schwartz, D. A. et al. Hofbauer cells and COVID-19 in pregnancy. *Arch. Pathol. Lab. Med.* **145**, 1328–1340 (2021).
45. Schwartz, D. A. et al. Chronic histiocytic intervillositis with trophoblast necrosis is a risk factor associated with placental infection from coronavirus disease 2019 (COVID-19) and intrauterine maternal-fetal severe acute respiratory syndrome coronavirus 2 (SARS-CoV-2) transmission in live-born and stillborn infants. *Arch. Pathol. Lab. Med.* **145**, 517–528 (2021).
46. Sun, Y. et al. Impact of maternal COVID-19 infection on offspring immunity and maternal-fetal outcomes at different pregnancy stages: a cohort study. *BMC Pregnancy Childbirth* **25**, 219 (2025).
47. Li, L. et al. Impact of Omicron BA.5 infection on maternal and neonatal outcomes. *Front. Cell. Infect. Microbiol.* **15**, 1551602 (2025).
48. Vogels, C. B. F. et al. Analytical sensitivity and efficiency comparisons of SARS-CoV-2 RT-qPCR primer-probe sets. *Nat. Microbiol.* **5**, 1299–1305 (2020).
49. Wölfel, R. et al. Virological assessment of hospitalized patients with COVID-2019. *Nature* **581**, 465–469 (2020).

Acknowledgements

The work was supported by the National Key Research and Development Program of China (2022YFC2702204 to L.J., 2022YFC2704702 to Z.W.), the National Natural Science Foundation of China (82271701 to L.J., 82071653 to L.J.), Shenkang Technology standardization management and promotion project (SHDC22023204 to L.J.), the Shanghai Science and Technology Project (23ZR1450400 to Z.W., 22ZR1480400 to Z.W.), Shanghai Municipal Health Commission (2024QN065 to S.W.), and the Shanghai Pudong New Area Health Commission Project (PW2022D-05 to L.J.). The funders had no role in study design, data collection and analysis, decision to publish or preparation of the manuscript. We are grateful for the technical support of Yuyu Xiong (KT Hua Hua) and Mengya Wang (KFBIO) on immunofluorescence and related analysis. We also thank the Applied Protein Technology for the support on Astral-DIA proteomic profiling. Sample storage was supported by the Department of Biobank, Shanghai First Maternity and Infant Hospital. BioRender was used in the preparation of Fig. 1a.

Author contributions

S.W., L.T., and Z.L. performed the experimental studies, analyzed data and wrote the original draft. M.W., X.H., S.S., Y.Z., K.L., Q.X., S.T., Z.Z., Y.X., and C.W. participated in sample collecting. F.Z. carried out the transmission electron microscopy. Z.W., L.J. designed and supervised this work, as well as edited the manuscript.

Competing interests

The authors declare no competing interests.

Additional information

Supplementary information The online version contains supplementary material available at https://doi.org/10.1038/s41467-025-65131-1.

Correspondence and requests for materials should be addressed to Zhiyun Wei or Liping Jin.

Peer review information *Nature Communications* thanks David Tingay, who co-reviewed with Georgie Dowse, and Daniele De Luca for their contribution to the peer review of this work. A peer review file is available.